KfK 3708
Februar 1984

Isoscalar Transition Rates of s-d Shell Nuclei Using a Modified Implicit Folding Procedure

D. K. Srivastava, H. Rebel
Institut für Kernphysik

Kernforschungszentrum Karlsruhe

KERNFORSCHUNGSZENTRUM KARLSRUHE
Institut für Kernphysik

KfK 3708

ISOSCALAR TRANSITION RATES OF s-d SHELL NUCLEI USING A MODIFIED IMPLICIT FOLDING PROCEDURE

D.K. Srivastava[+] and H. Rebel

Kernforschungszentrum Karlsruhe GmbH, Karlsruhe

[+] On leave from Variable Energy Cyclotron Centre, Calcutta

Als Manuskript vervielfältigt
Für diesen Bericht behalten wir uns alle Rechte vor

Kernforschungszentrum Karlsruhe GmbH
ISSN 0303-4003

ABSTRACT

Elastic and inelastic scattering data for 104 MeV alpha-particles from $^{20,22}Ne$, $^{24,26}Mg$, ^{28}Si and ^{32}S have been analysed in a coupled channels approach assuming a Woods-Saxon and a Woods-Saxon squared shape for the real potential. The isoscalar transition rates for the $\Delta L = 2$ and $\Delta L = 4$ transitions are evaluated using the implicit folding procedures.

ISOSKALARE ÜBERGANGSRATEN VON S-D-SCHALENKERNEN NACH EINEM MODIFIZIERTEN FALTUNGSMODELL

Elastische und unelastische Streudaten für 104 MeV Alpha-Teilchen an $^{20,22}Ne$, $^{24,26}Mg$, ^{28}Si und ^{32}S wurden mit der Methode der gekoppelten Kanäle analysiert, wobei eine Woods-Saxon wie auch eine quadratische Woods-Saxon-Form untersucht wurde. Isoskalare Übergangsraten wurden für $\Delta L = 2$ und $\Delta L = 4$ Übergänge gewonnen, wobei implizite Faltungsprozeduren benutzt wurden.

1. INTRODUCTION

Implicit folding procedures [1] for the determination of isoscalar transition rates of nuclei from the transition-potentials obtained phenomenologically, would have been one of the most elegant methods for these evaluations *if the underlying nuclear forces were not density-dependent*. However, it is by now very well established that the density-dependence of the nuclear forces can not be overlooked in any meaningful and quantitative study of nuclear reactions. This is especially so, for elastic and inelastic scattering where very good quality data extending to large angles are now becoming available.

In an earlier work [2], we modified the implicit (single) folding procedure (MIFP) for application to the analysis of alpha particle inelastic scattering from nuclei. In this work we apply MIFP to the specific example of s-d shell nuclei. We also study the suitability of a (deformed) WS-square potential form for the real potential for the description of elastic and inelastic scattering data of these light nuclei.

2. ANALYSIS

For the present study, we use the elastic and inelastic scattering data for 104 MeV alpha-particle from N = Z nuclei, ^{20}Ne, ^{24}Mg, ^{28}Si and ^{32}S and N = Z + 2 nuclei. ^{22}Ne and ^{26}Mg, measured earlier at the Karlsruhe Isocronous Cyclotron [3]. The inelastic scattering data include the results for the 1·63 MeV (2^+_1) and the 4.25 MeV (4^+_1) levels for ^{20}Ne, the 1.28 MeV (2^+_1) and the 3.34 MeV (4^+_1) levels for ^{22}Ne, the 1.37 MeV (2^+_1) and the 4.12 MeV (4^+_1) levels for ^{24}Mg, the 1.81 MeV (2^+_1) level for ^{26}Mg, the 1.78 MeV (2^+_1) and the 4.61 MeV (4^+_1) levels for ^{28}Si and the 2.24 MeV (2^+_1) level for ^{32}S.

The analysis was performed assuming symmetric rotational model description for all the nuclei, even though there are indications that ^{24}Mg is a triaxial nucleus [4] and that ^{32}S can be more adequately described as a vibrational nucleus [5]. We have retained the symmetrical rotational frame-work for these two as it is known

to give fits of similar quality [3,5].

A $0^+ - 2^+ - 4^+$ coupling scheme has been used when the data include results for the 4^+ state. For ^{26}Mg and ^{32}S $0^+ - 2^+$ coupling-scheme has been used along with the assumption that $\beta_4 = 0$. The coupled-channel code ECIS-79 by Raynal [6] has been used for the analysis.

The real part of the potential was assumed to be of a Woods-Saxon or a Woods-Saxon square shape, where as the imaginary potential was always taken to be of Woods-Saxon shape. A homogeneous (deformed) charge distribution was assumed for the calculation of the Coloumb potential, having a reduced radius 1 • 30 fm.

The deformation parameters, β_2 and β_4 (eq.2.1, below), were taken to be equal for the real, imaginary and the Coloumb potentials. This was done primarily to keep the number of parameters to a minimum. We also feel, that, as we search on all parameters of the imaginary potential, any deficiency due to this assumption would be absorbed by the adjustments of other parameters.

The radii appearing in all the potentials considered were taken to ge deformed as

$$R(\theta,\phi) = r_o \cdot A^{1/3}[1 + \beta_2 Y_{20}(\theta,\phi) + \beta_4 Y_{40}(\theta,\phi)] \qquad (2.1)$$

Terms up to L = 10 were considered in the multipole expansion of the deformed optical potential.

The reanalysis of the earlier data was prompted by the following reasons.

1.) The results for coupled-channel analysis reported earlier [3] were obtained by fitting data only up to 60°, and now we know that even data at just a few points at larger angles can be decisive in eliminating ambiguities.
2.) The earlier analysis [3] was performed by assigning a uniform error at all the angles.

In this work, we assign actual errors at all the points, retain higher angle data whenever available while analysing the elastic and inelastic scattering data.

3. RESULTS

In tables 1 and 2, we give the best fit-parameters for the Real WS-Imaginary WS and Real WS^2-Imaginary WS parametrizations for the potentials. When the data considered did not extend to angles large enough for the elimination of parameter ambiguities (as for ^{32}S) we have given results which are closest to the physical families having a depth of about 100 MeV for the real (WS) potential.

A perusal of the Tables 1 and 2 reveals that both shapes, WS as well WS^2, for the real potential give almost similar fits to the elastic and inelastic scattering data under consideration, even though a slight preference for the WS^2-shape is discernible as the mass-number increases. For ^{20}Ne and ^{22}Ne nuclei the WS-shape is somewhat preferred. Fits to the experimental data are given in figs. 1-6.

We also notice that the β_2 values for the WS^2-shape (from table 2) are almost always slightly smaller than the corresponding values for the WS-shape, though not very different. This aspect is a good indication for the usefulness of β_2 as a "measure" of the deviation of the deformed potential from a spherical shape.

It is also interesting to note that the potential depth for the real potential for ^{28}Si is smaller than the same for its neighbouring nuclei by about 10 %. The results for ^{32}S are less conclusive due to the restricted angular range of the data. It should be reasonable to associate this observation with the fact that ^{28}Si is found to be having an oblate shape. We feel that this can be taken to indicate that the higher order corrections to the real optical potential effected by the coupling depend upon the sign of the deformation.

4. RADIAL MOMENT ANALYSIS OF THE TRANSITION POTENTIALS

In order to get results for the isoscalar transition rates of the excitations considered here, we have to translate the information about the transition potentials obtained here to the corresponding quantities about the wavefunctions (densities) of the nuclei. This can be achieved easily by the use of the Satchler's theorem [7],

provided the true (experimentally observed) interaction potential $V(\vec{r}_\alpha)$ is really generated by a single folding procedure, such that,

$$V(\vec{r}_\alpha) = \int \rho(\vec{r})\ V_{eff}(|\vec{r}_\alpha - \vec{r}|)\ d\vec{r} \tag{4.1}$$

and the effective alpha-nucleon force is central and density independent. For such cases, one has [1]

$$\frac{q^V_{LM}}{J_V} = \frac{q^\rho_{LM}}{J_\rho} \tag{4.2}$$

where

$$q^f_{LM} = \int f(\vec{r})\ r^L\ Y_{LM}(\Omega)\ d\vec{r} \tag{4.3}$$

and

$$J_f = \int f(\vec{r})\ d\vec{r} \tag{4.4}$$

and therefore the isoscalar transition rate of the excitation, which is proportional to the square of multipole moment of the "deformed" density is easily obtained from the normalized multipole moment of the potential.

It may also be recalled here, that, under the assumption of identical deformation for the neutron and the proton distributions the $B(EL, 0^+ \to L^+)$ value is given by

$$B(EL,\ 0^+ \to L^+) = e^2\ \left[\frac{Z}{A}\ q^\rho_{L0}\right]^2 \text{ in } e^2\ fm^{2L} \tag{4.5}$$

This assumption should be quite justified for light nuclei having N = Z. Even for nuclei having $N \neq Z$, the fact that the p-n force is much stronger than the p-p or the n-n force, would necessitate that the neutron distribution closely follows the proton distribution.

Thus the experimental results for the B(EL) values can be used to get q^ρ_{L0} in a "model-independent" fashion for comparison with the results obtained by using the implicit folding procedure (IFP), given by (4.2) above.

In table 3, we give the results for such a "radial moment analysis" using IFP. A comparison of these values with those obtained from electromagnetic procedures etc. are given in table 4.

We would like to emphasize here that we have not included such results for q^{ρ}_{20} and q^{ρ}_{40} in the table 4, which were obtained in a DWBA analysis of the (α,α') data, as these do not include the effects of multiple excitations. We have also not included results from (p,p') or (^{3}He, ^{3}He') anlysis as protons and ^{3}He do not interact act equally strongly with protons and neutrons as alpha-particles do, and thus the results for the nuclear deformations derived from these analyses should not be compared.

We immediately notice that (q^{V}_{20}/J_V) is an accurately determined quantity in a coupled channels analysis of the inelastic scattering data, for a given nucleus. This of course is an important requirement for the applicability of the IFP and it is gratifying to note that it is met rather nicely for the $\Delta L = 2$ transition.

The corresponding value for the (q^{V}_{L0}/J_V) for the $\Delta L = 4$ transition undergoes a rather large change when the shape of the potential is changed. As the fits to the cross section are of similar quality, this variation could be ascribed to the uncertainties in the data and the possible inadequacy of the extended optical model in describing transitions of a higher multipolarity. It should be remarked that a simultaneous description of the 0^+, 2^+ and 4^+ data in a coupled channels approach for high energy alpha particles, using a single deformed potential is a fairly tough requirement.

It is also felt that if exchange effects are large and L-dependent as in the case of nucleon inelastic scattering, say, the ordinary collective model form-factor assumed in this work would be inadequate, expecially for transitions of higher multipolarities at higher energies. One way out of this impasse could be to perform analysis of the data with the addition of a Fourier-Bessel series to the potential which would provides realistic error estimates and also lift the constraints imposed due to a presupposed shape of the potential [8].

From Table 4, we find that q^{ρ}_{20} determined from IFP is in quite good agreement with the values obtained using the B(E2) results. This is in confirmity with our earlier findings [2] that the corrections to the IFP for density dependence of the alpha-nucleon force are small for L = 2, making IFP fairly accurate for these transitions.

However, the results for q^{ρ}_{40} using the IFP are almost always too large compared to the values obtained from electromagnetic means.

In the light of our recent work [2], we feel that at least part of this discrepancy could be ascribed to the density-dependence of the alpha-nucleon force. Thus if the effective alpha-nucleon force v_{eff} in (4.1) is density dependent

$$V_{eff}(\vec{r}_{\alpha},\vec{r}) = [1-\gamma\ \rho^{2/3}(\vec{r})]v_{o}(|\vec{r}_{\alpha}-\vec{r}|) \tag{4.6}$$

than, one can show that [2]

$$\frac{q^{V}_{LM}}{J_{V}} = \frac{q^{\rho}_{LM}}{J_{\rho}} \cdot C_{LM} \tag{4.7}$$

with

$$C_{LM} = [1-\gamma\ (M_{LM}/q^{\rho}_{LM})]\ /\ [1-\gamma\ K/_{A}] \tag{4.8}$$

where

$$M_{LM} = \int \rho^{5/3}(\vec{r})\ r^{L}\ Y_{LM}(\Omega)\ d\vec{r} \tag{4.9}$$

$$K = \int \rho^{5/3}(\vec{r})\ d\vec{r} \tag{4.10}$$

and

$$J_{\rho} = A \tag{4.11}$$

For small values of deformations, it was shown [2] that C_{LM} was independent of deformation and its values were tabulated for a set of representative nuclei.

Though we can not say that the deformations we observe in tables 1 and 2 are small, we can use the correction factors C_{L} given in table (A.2) of ref. 2 to see the improvement obtained in the values of q^{ρ}_{L0}.

The values for thus modified implicit folding procedure are given in table 4. We find an improved agreement between the q^{ρ}_{40}(MIFP) and q^{ρ}_{40}(em) without substantially disturbing the good agreement for the q^{ρ}_{20} values obtained earlier.

However, it should be realized that the full-correction for the density-dependence of the alpha-nucleon force can be obtained only by an iterative solution of (4.7) and (4.8). We feel it

should be more direct and revealing to perform an explicit folding model calculation in such situation [9].

5. SUMMARY AND CONCLUSIONS

In brief, we have analysed the elastic and inelastic scattering data for s-d shell nuclei for 104 MeV alpha-particle in a coupled-channels approach using a symmetric rotational picture for the nuclei. A WS and a WS^2 shape has been used for the real part of the potential. Though fits of similar quality are obtained for both the shapes a slight preference for the WS^2 shape is discernible as the mass-number increases.

The isoscalar transition rates for the $\Delta L = 2$ transitions determined using the conventional IFP are in good agreement with the same determined from electromagnetic means whereas those for $\Delta L = 4$ are a bit two high. Corrections for the density dependence of the alpha-nucleon force, as suggested by us earlier [2] provided improved agreement for these.

ACKNOWLEDGEMENTS

Useful discussions with Dr. H.J. Gils and Dr. J. Albiński are thankfully acknowledged.

REFERENCES

1. H. Rebel, Z. Phys. A277 (1976) 35

2. D.K. Srivastava and H. Rebel, KfK-3586 and to appear in Z. Phys. A.

3. H. Rebel, G.W. Schweimer, G. Schatz, J. Specht, R. Lohken, G. Hauser, D. Habs and H. Klewe-Nebenius, Nucl. Phys. A182 (1972) 145, G.W. Schweimer, H. Rebel, G. Nowicki, G. Hauser and R. Löhken, Phys. Lett. 39B (1972) 627

4. See e.g. G.S. Blanpied et al., Phys. Rev. C25 (1982) 422 and ref. therein.

5. See e.g., R. de Swiniarski, F.G. Resmini, D.L. Hendrie and A.D. Bacher, Nucl. Phys. A261 (1976) 111, and ref. therein

6. J. Raynal, private communication

7. G.R. Satchler, J. Math. Phys. 13 (1972) 1118

8. V. Corcalciuc, H. Rebel, R. Pesl and H.J. Gils, J. Phys. G. Nucl. Phys. 9 (1983) 177

9. D.K. Srivastava and H. Rebel, KfK preprint in preparation

Table 1 Best fit coupled-channels parameters assuming a WS-shape for the real as well as the imaginary potential.

Nucleus	V_o MeV	r_V fm	a_V fm	W_o MeV	r_W fm	a_W fm	β_2 -	β_4 -	χ^2/F -	Remarks (coupling)
^{20}Ne	98.72	1.369	o.748	15.25	1.827	o.459	o.338	o.1o6	7.8o	$o^+-2^+-4^+$
^{22}Ne	1o7.89	1.252	o.791	15.19	1.729	o.615	o.359	o.o16	13.8o	$o^+-2^+-4^+$
^{24}Mg	1o8.52	1.241	o.751	2o.55	1.511	o.829	o.372	o.o1o	38.1o	$o^+-2^+-4^+$
^{26}Mg	1o2.11	1.3o5	o.718	25.79	1.48o	o.748	o.268	-	39.5o	o^+-2^+
^{28}Si	91.68	1.435	o.617	26.66	1.52o	o.587	-o.282	o.o9o	3.12	$o^+-2^+-4^+$
^{32}S	96.37	1.514	o.544	24.24	1.494	o.686	o.2o8	-	19.81	o^+-2^+

Table 2 Best fit coupled-channels parameters assuming a WS^2-shape for the real potential and a WS-shape for the imaginary potential.

Nucleus	V_o (MeV)	r_V fm	a_V fm	W_o MeV	r_w fm	a_W fm	β_2 -	β_4 -	χ^2/F -	Remarks (coupling)
^{20}Ne	159.05	1.395	1.350	12.42	1.891	0.460	0.336	0.095	8.87	$0^+-2^+-4^+$
^{22}Ne	143.22	1.424	1.268	16.38	1.651	0.734	0.328	0.024	16.97	$0^+-2^+-4^+$
^{24}Mg	154.81	1.346	1.257	20.792	1.438	0.938	0.346	0.029	34.93	$0^+-2^+-4^+$
^{26}Mg	137.55	1.431	1.170	32.99	1.271	0.928	0.256	-	33.30	0^+-2^+
^{28}Si	123.19	1.520	1.056	23.93	1.500	0.662	-0.275	0.085	2.97	$0^+-2^+-4^+$
^{32}S	113.79	1.605	0.960	20.02	1.573	0.679	0.192	-	19.05	0^+-2^+

Table 3 Multipole moments q^{ρ}_{LO} of the density distribution obtained using the Implicit Folding Procedure (IFP) (Eq. 4.2)

Nucleus	Shape of $V(\vec{r}_\alpha)$	$J_V/4A$ MeV.fm^3/ nucleon pair	$q^{\rho}_{20} = A \cdot \frac{q^V_{20}}{J_V}$ fm^2	$q^{\rho}_{40} = A \cdot \frac{q^V_{40}}{J_V}$ fm^4
^{20}Ne	WS	379.6	35.50	557.34
	WS^2	357.8	34.88	511.20
^{22}Ne	WS	340.1	36.14	240.00
	WS^2	330.0	37.21	287.25
^{24}Mg	WS	318.9	41.21	254.83
	WS^2	303.5	41.22	332.04
^{26}Mg	WS	322.7	35.58	142.58
	WS^2	310.2	35.32	150.66
^{28}Si	WS	345.7	-41.28	537.77
	WS^2	330.4	-41.03	513.80
^{32}S	WS	377.5	43.89	182.44
	WS^2	358.1	41.89	169.26

Table 4a Deformation of s-d shell nuclei from different studies

^{20}Ne

Projectile	Method	q^{ρ}_{20} fm^2	q^{ρ}_{40} fm^4	Ref.
1o4 MeV α	IFP, WS	35.5O	557.34	This work
	IFP, WS^2	34.88	511.2o	This work
	MIFP, WS	32.87	459.47	This work
	MIFP, WS^2	32.36	421.43	This work
	DI, FOLD	36.O2	422.56	a
	DD, FOLD	32.25	161.23	a
-	B(EL)	34.o6	391.6	b
	B(EL)	37.42	-	c
(e,e')	-	36.6o	256.6	d
$^{2o8}Pb+^{2o}Ne$ (131 MeV)	-	36.63	268.1	e
Pt + ^{2o}Ne (91 MeV)	-	38.47	-	f

Table 4b Deformation of s-d shell nuclei from different studies

^{22}Ne

Projectile	Method	q^{ρ}_{20} fm^2	q^{ρ}_{40} fm^4	Ref.
1o4 MeV α	IFP, WS	36.14	24o.oo	This work
	IFP, WS^2	37.21	287.25	This work
	MIFP, WS	33.48	197.21	This work
	MIFP, WS^2	34.47	236.o3	This work
	DI, FOLD	36.55	268.97	a
	DD, FOLD	32.64	164.83	a
-	B(EL)	33.94	-	b
-	B(EL)	34.o8	-	c
Pt + ^{22}Ne (91 MeV)	-	35.47	-	f

Table 4c Deformation of s-d shell nuclei from different studies

$^{24}_{Mg}$

Projectile	Method	q^{ρ}_{20} fm^2	q^{ρ}_{40} fm^4	Ref.
1o4 MeV, α	IFP, WS	41.21	254.88	This work
	IFP, WS^2	41.22	332.o4	This work
	MIFP, WS	38.12	2o8.71	This work
	MIFP, WS^2	38.13	271.94	This work
	DI, FOLD	4o.41	89.23	a
	DD, FOLD	35.93	157.o2	a
-	B(EL)	41.56	114.o7	b
-	B(EL)	41.47	-	c
(e,e')	-	42.24	-	q

Table 4d Deformation of s-d shell nuclei from different studies

^{26}Mg

Projectile	Method	q^{ρ}_{20} fm^2	q^{ρ}_{40} fm^4	Ref.
104 MeV, α	IFP, WS	35.58	142.58	This work
	IFP, WS^2	35.32	15o.66	This work
	MIFP, WS	32.9o	116.53	This work
	MIFP, WS^2	32.66	123.14	This work
	DI, FOLD	31.63	114.71	a
	DD, FOLD	28.93	94.42	a
-	B(EL)	37.36	416.26	b
-	B(EL)	41.68	-	c

Table 4e Deformation of s-d shell nuclei from different studies

^{28}Si

Projectile	Method	q^{ρ}_{20} fm^2	q^{ρ}_{40} fm^4	Ref.
104 MeV, α	IFP, WS	-41.28	537.77	This work
	IFP, WS^2	-41.o3	513.8o	This work
	MIFP, WS	-38.15	438.64	This work
	MIFP, WS^2	-37.92	419.o9	This work
	DI, FOLD	-34.95	313.62	a
	DD, FOLD	-33.64	151.63	b
-	B(EL)	36.24	268.26	b
-	B(EL)	35.78	-	c
(e.e')		37.o9	266.o	g

Table 4f Deformation of s-d shell nuclei from different studies

^{32}S

Projectile	Method	q^{ρ}_{20} fm^2	q^{ρ}_{40} fm^4	Ref.
104 MeV, α	IFP, WS	43.89	182.44	This work
	IFP, WS^2	41.89	169.26	This work
	MIFP, WS	4o.56	148.44	This work
	MIFP, WS^2	38.72	137.72	This work
	DI, FOLD	33.44	1o3.39	a
	DD, FOLD	32.53	98.34	a
-	B(EL)	34.74	-	b
-	B(EL)	33.47	-	c

IFP = Implicit Folding Procedure
WS/WS^2 = Real potential has WS/WS^2 shape
MIFP = IFP, modified for density-dependence of the alpha-nucleon force
DI,FOLD= Real part by folding density-independent alpha-nucleon force
DD,FOLD= Real Part by folding density-dependent alpha-nucleon force.

a D.K. Srivastava and H. Rebel, to be published (Ref.9)

b P.M. Endt, Atomic Data and Nuclear Data Tables 23 (1979) 3.

c A. Christy and O. Häusser, Nucl. Data Tables 11 (1972) 11.

d Y. Horikawa, Y. Torizuka, A. Nakada, S. Mitsunobu, Y. Kojima and M. Kimura, Phys. Lett. 36B (1979) 9.

e E.E. Gross, T.P. Cleary, J.L.C. Ford, D.C. Hensley and K.S. Toth, Phys. Rev. C17(1978) 1665.

f D.K. Olsen, W.R. Philipps and A.R. Barnett, Phys. Lett. 39B (1972) 201.

g A. Nakada and Y. Torizuka, J. Phys. Soc. (Japan) 32 (1972) 1.

Figure Captions

Fig. 1 - 6 Elastic and inelastic scattering data for 104 MeV alpha-particles, fitted in a coupled channels analysis.

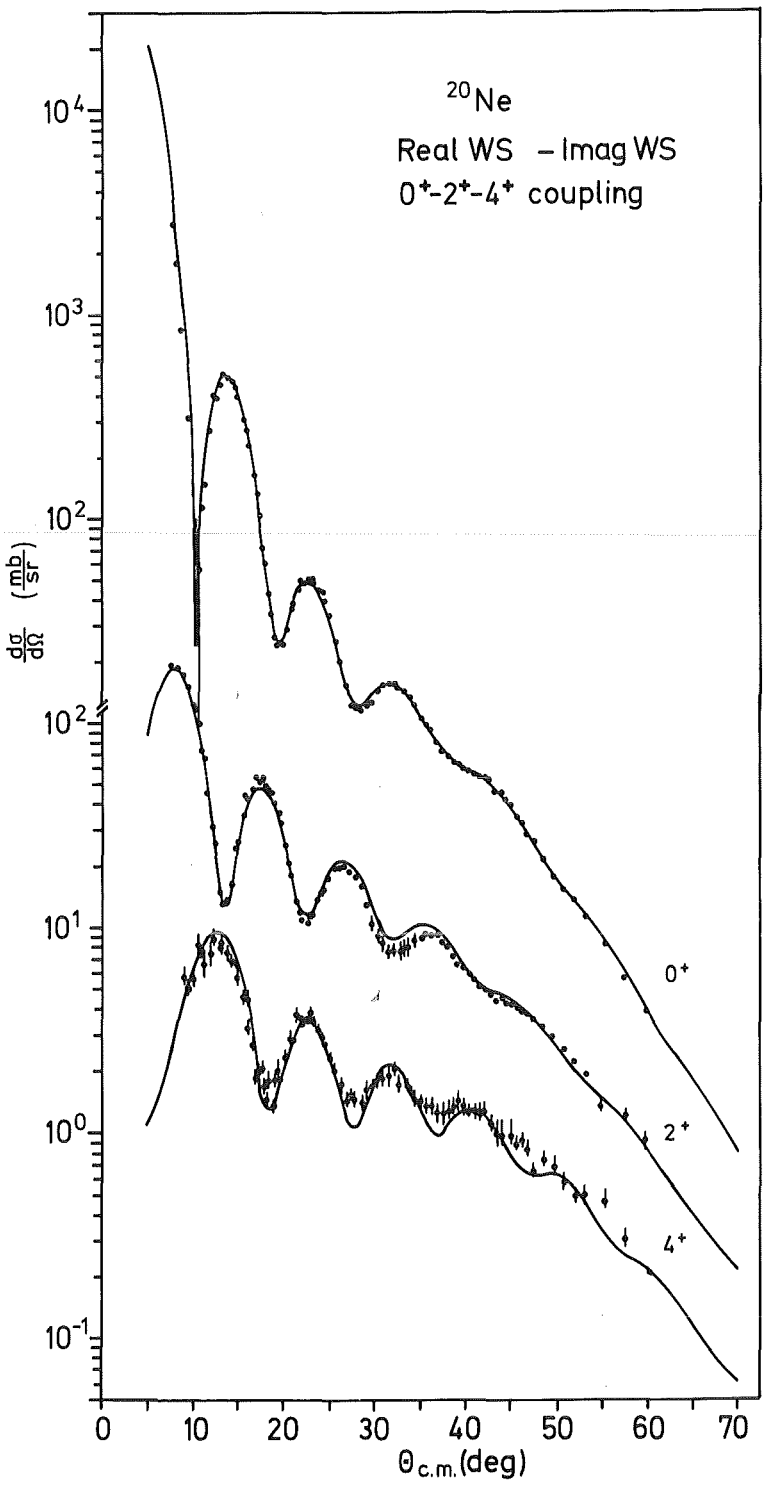
^{20}Ne
Real WS – Imag WS
0^+-2^+-4^+ coupling
10^4
10^3
10^2
10^2
10^1
10^0
10^{-1}
$\frac{d\sigma}{d\Omega}$ $(\frac{mb}{sr})$
0^+
2^+
4^+
0
10
20
30
40
50
60
70
$\Theta_{c.m.}$(deg)

Fig. 1

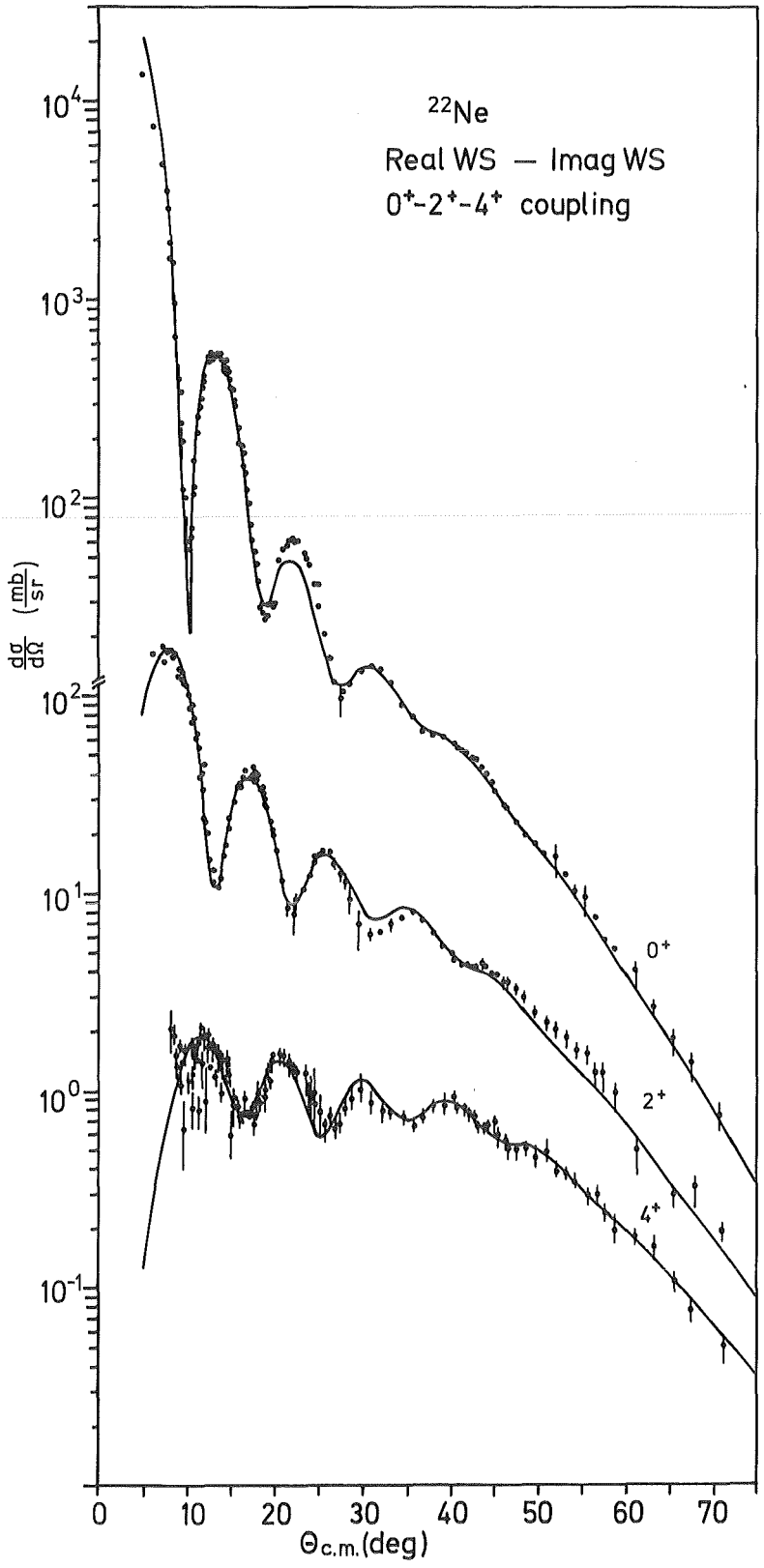
^{22}Ne
Real WS — Imag WS
0^+-2^+-4^+ coupling
10^4
10^3
10^2
10^2
10^1
10^0
10^{-1}
$\frac{d\sigma}{d\Omega}$ $(\frac{mb}{sr})$
0^+
2^+
4^+
0
10
20
30
40
50
60
70
$\Theta_{c.m.}$(deg)

Fig. 2

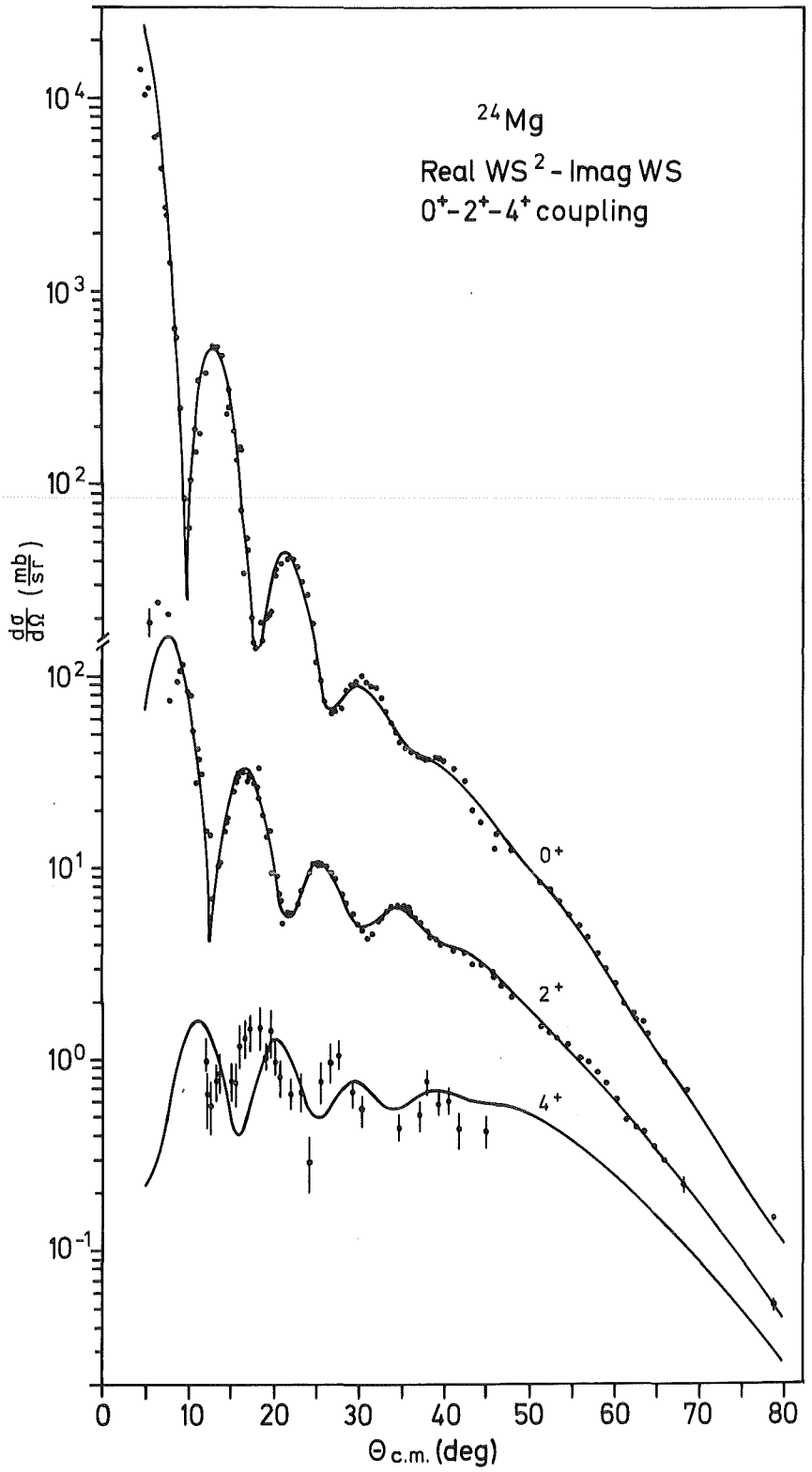
^{24}Mg
Real WS^2 - Imag WS
0^+-2^+-4^+ coupling
10^4
10^3
10^2
10^2
10^1
10^0
10^{-1}
$\frac{d\sigma}{d\Omega}$ ($\frac{mb}{sr}$)
0^+
2^+
4^+
0
10
20
30
40
50
60
70
80
$\Theta_{c.m.}$ (deg)

Fig. 3

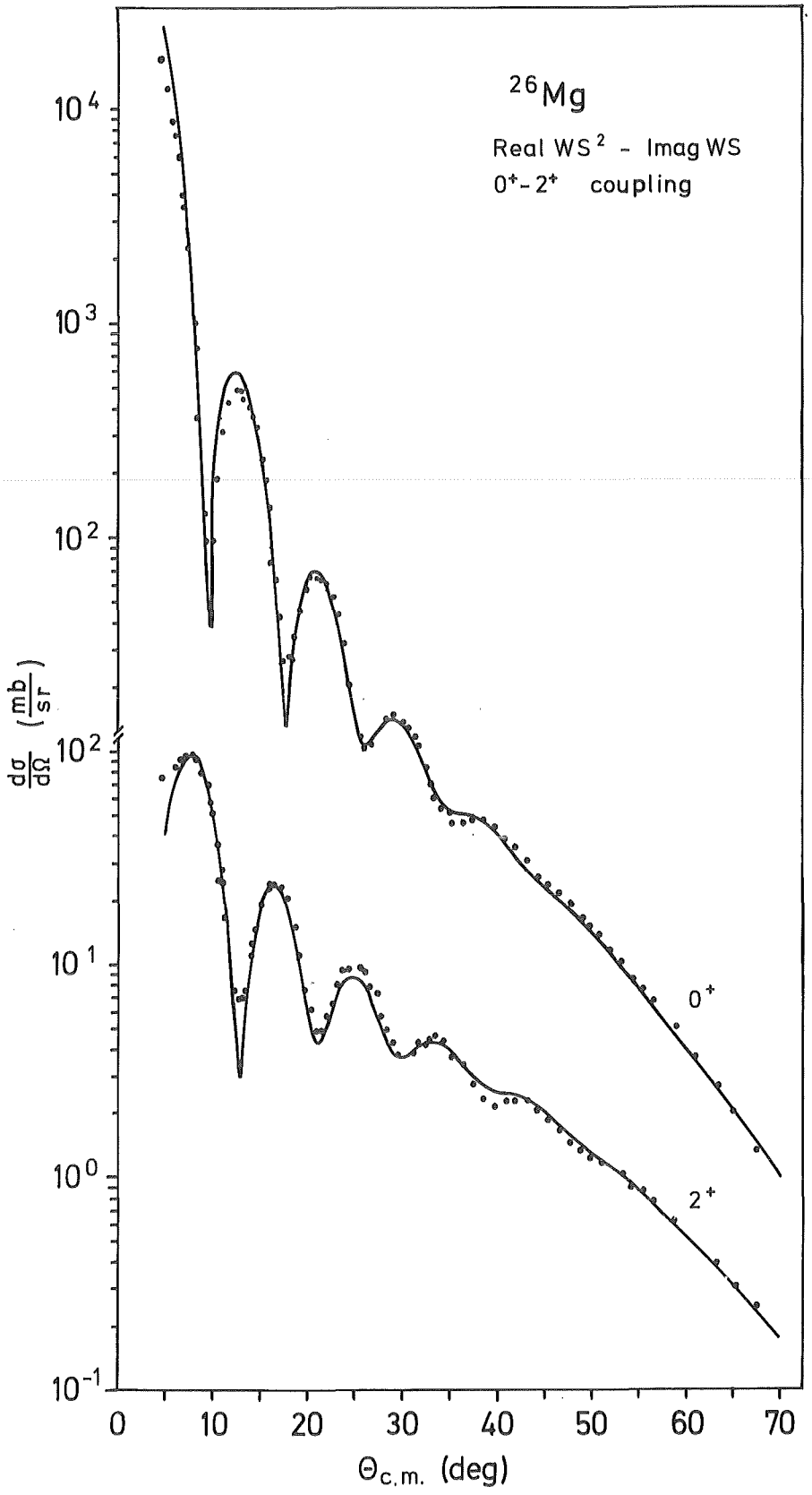
^{26}Mg
Real WS^2 - Imag WS
0^+-2^+ coupling
10^4
10^3
10^2
10^2
10^1
10^0
10^{-1}
$\frac{d\sigma}{d\Omega}$ $(\frac{mb}{sr})$
0^+
2^+
0
10
20
30
40
50
60
70
$\Theta_{c.m.}$ (deg)

Fig. 4

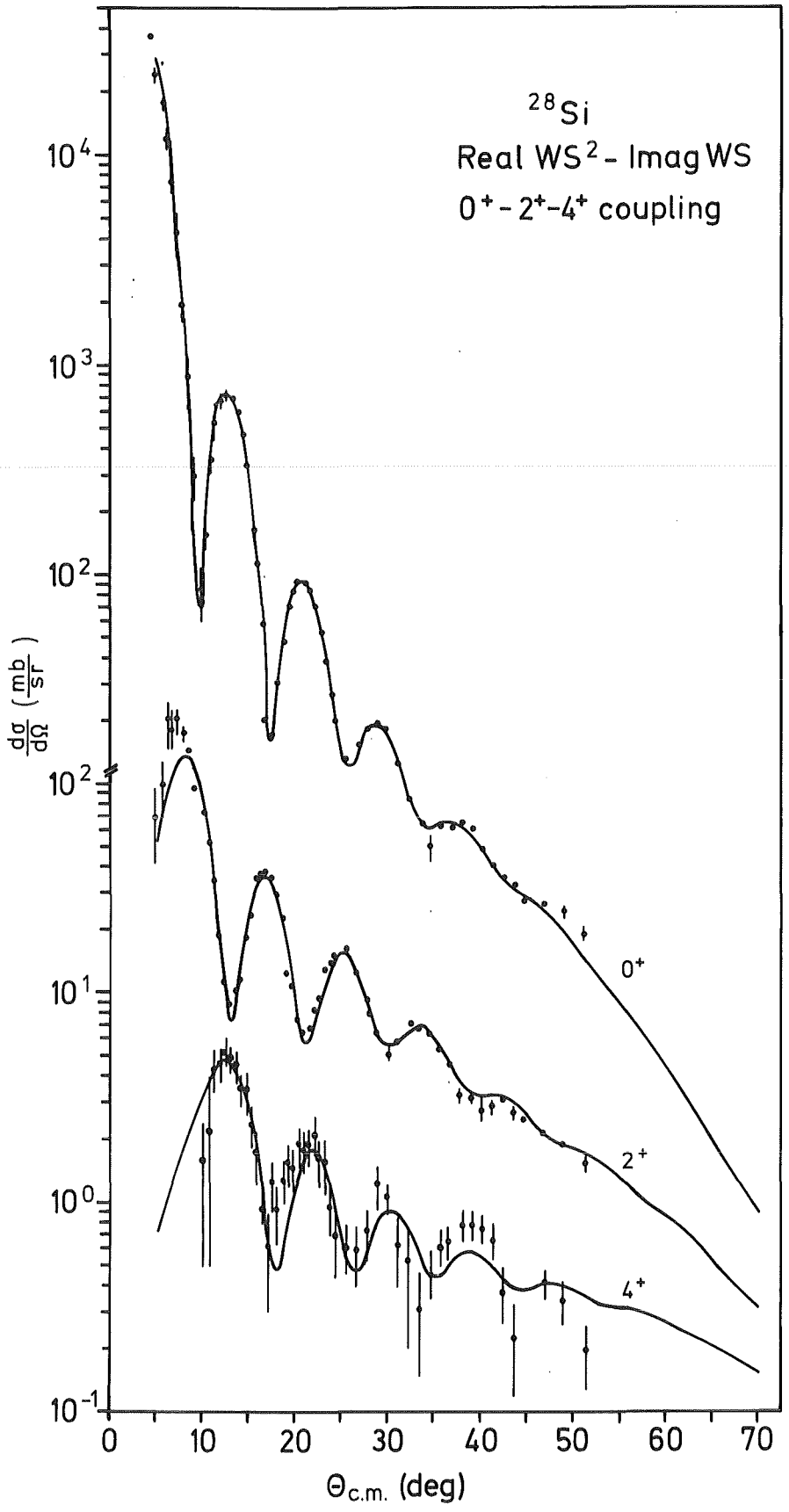
^{28}Si
Real WS^2 - Imag WS
$0^+ - 2^+ - 4^+$ coupling
10^4
10^3
10^2
10^2
10^1
10^0
10^{-1}
$\frac{d\sigma}{d\Omega}$ ($\frac{mb}{sr}$)
0^+
2^+
4^+
0
10
20
30
40
50
60
70
$\Theta_{c.m.}$ (deg)

Fig. 5

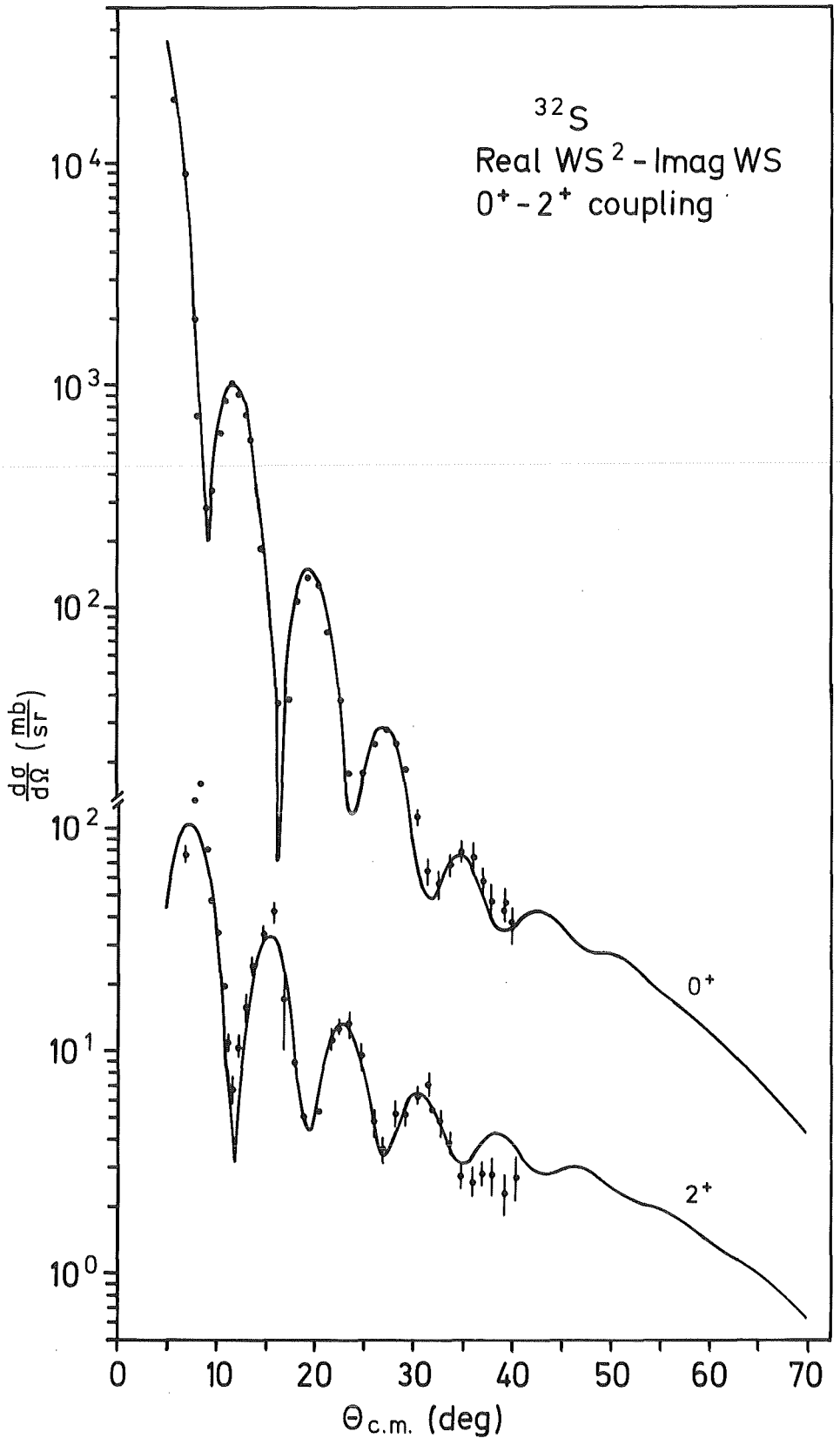
^{32}S
Real WS^2 - Imag WS
$0^+ - 2^+$ coupling
10^4
10^3
10^2
10^2
10^1
10^0
$\frac{d\sigma}{d\Omega}$ ($\frac{mb}{sr}$)
0^+
2^+
0
10
20
30
40
50
60
70
$\Theta_{c.m.}$ (deg)

Fig. 6